Article

Effect of Ti Atoms on Néel Relaxation Mechanism at Magnetic Heating Performance of Iron Oxide Nanoparticles

Musa Mutlu Can [1,*], Chasan Bairam [1], Seda Aksoy [2], Dürdane Serap Kuruca [3], Satoru Kaneko [4,5,6], Zerrin Aktaş [7] and Mustafa Oral Öncül [8]

1   Renewable Energy and Oxide Hybrid Systems Laboratory, Department of Physics, Faculty of Science, Istanbul University, Istanbul 34314, Turkey; chasanbairam@gmail.com
2   Department of Physics Engineering, Istanbul Technical University, Istanbul 34469, Turkey; sedaksoy@gmail.com
3   Department of Physiology, Faculty of Medicine, Istanbul University, Istanbul 34390, Turkey; sererdem@yahoo.com
4   National Cheng Kung University, Tainan 701, Taiwan; kaneko.s.al@m.titech.ac.jp
5   Electronics Engineering Department, Kanagawa Institute of Industrial Science and Technology (KISTEC), Ebina 243-0435, Kanagawa, Japan
6   Tokyo Institute of Technology, Nagatsuta, Yokohama 226-8502, Kanagawa, Japan
7   Faculty of Medicine, Department of Clinical Microbiology, Istanbul University, Istanbul 34390, Turkey; zaktas@istanbul.edu.tr
8   Faculty of Medicine, Department of Infectious Diseases and Clinical Microbiology, Istanbul University, Istanbul 34390, Turkey; oraloncul@yahoo.com
*   Correspondence: musa.can@istanbul.edu.tr; Tel.: +090-(533)-929-0718

Abstract: The study was based on understanding the relationship between titanium (Ti) doping amount and magnetic heating performance of magnetite (Fe_3O_4). Superparamagnetic nanosized Ti-doped magnetite ((Fe_{1-x},Ti_x)$_3$$O_4$; x = 0.02, 0.03 and 0.05) particles were synthesized by sol-gel technique. In addition to (Fe_{1-x},Ti_x)$_3$$O_4$ nanoparticles, SiO_2 coated (Fe_{1-x},Ti_x)$_3$$O_4$ nanoparticles were produced as core-shell structures to understand the effects of silica coating on the magnetic properties of nanoparticles. Moreover, the magnetic properties were associated with the Néel relaxation mechanism due to the magnetic heating ability of single-domain state nanoparticles. In terms of results, it was observed that the induced RF magnetic field for SiO_2 coated ($Fe_{0.97}$,$Ti_{0.03}$)$_3$$O_4$ nanoparticles caused an increase in temperature difference (ΔT), which reached up to 22 °C in 10 min. The ΔT values of SiO_2 coated ($Fe_{0.97}$,$Ti_{0.03}$)$_3$$O_4$ nanoparticles were very close to the values of uncoated Fe_3O_4 nanoparticles.

Keywords: oxide semiconductor; point defects; Néel relaxation; magnetic hyperthermia; superparamagnetic nanoparticles

1. Introduction

The crystal structure of magnetite (Fe_3O_4) has a spinel cubic structure with Fd-3m space group [1,2]. Fe_3O_4 crystal structures obtain tetrahedral and octahedral sublattices, occupied by Fe^{2+} and Fe^{3+} cations coordinated with 32 oxygen atoms [1,2]. Ferrimagnetic properties are governed by the coupling of cation spins in octahedral and tetrahedral sites [1,2]. Properties, such as low toxicity, suitable magnetic properties, and easy fabrication, make the ferrite particles suitable for hyperthermia usages [3]. Each magnetic domain in a magnetic nanoparticle is oriented along the direction of the externally applied magnetic field. Also, especially for single-domain magnetic nanoparticles, all particles can be oriented in the direction of the magnetic field (Brownian motion), and the magnetic domains inside a particle can rotate without rotating the magnetic particle (Neel motion) [4]. In both cases, due to the desire to be in line with the external magnetic field, alternating magnetic fields initiate heating in and around single-domain magnetic particles.

During the last few decades, magnetic hyperthermia has become a widely researched topic (especially for cancer treatments) [5–11]. In recent technological applications, ferrite nanoparticles have emerged as the most popular candidate for magnetic hyperthermia applications. The heating performance of magnetic nanoparticles is investigated mainly depending on size and magnetic domain number in the particle [12]. The heating performance of multi-domain magnetic nanoparticles is related to energy losses from magnetic hysteresis due to the domain wall motions and eddy currents induced in magnetic grains [12,13]. Unlike multidomain nanosized particles, the magneto-heating performance of single magnetic domain nanosized particles is mainly correlated with magnetic anisotropy, inter/intra particles interactions and homogeny distributed magnetic nanoparticles [14]. Magnetic relaxation is generally the dominant mechanism in magnetic anisotropy and thus in magneto heating performance of nanoparticles. The magneto-heating performance of single magnetic domain nanosized particles is associated with two mechanisms, Néel and Brownian relaxations [15–17]. Brownian motion is created by mechanical fluctuation that performing by an entire nanoparticle rotating its own axis. On the other hand, the Néel relaxation mechanism is independent from the rotational motion of particles. The internal flip of spins with respect to the crystalline lattice creates magnetic heating associated with Néel relaxation [18–20]. Both relaxation mechanisms cause an increase in the temperature of magnetic nanoparticles. Even though magneto-heating can be observed with temperature increase, the magneto-heating performance of magnetic nanoparticles can be measured by specific absorption rate (SAR) values. SAR values can be defined by absorbed/converted magnetic energy into thermal energy and in technological applications (especially in cancer treatments) mainly modified properties of magnetic nanoparticles [3]. For magnetic hyperthermia applications, Néel relaxation has certain advantages due to its high SAR values [3]. On the other hand, Brownian relaxation is largely dependent on the viscosity of the medium surrounded by particles, and in cancer treatment SAR value is not enough for magneto-heating processes [3]. Liquid environmental conditions, such as different viscosities of the medium, agglomeration of nanoparticles within different cells, or fixation of nanoparticles in cell membranes (or extracellular tissue), weaken or inhibit the mechanical rotation of magnetic nanoparticles [21]. During the cancer treatments, due to the lack of movement or fluctuation of magnetic nanoparticles inside cancer cells Néel relaxation became the dominant factor for magnetic heating in compare to Brownian movement [3,20,21].

The study is based on the evaluation of the magneto heating performance of individual, non-interacting, and monodisperse particles in highly viscous environments confirming the Néel relaxation mechanism. The magneto heating mechanism is investigated for superparamagnetic Fe_3O_4 nanoparticles doped with Ti atoms. The magneto heating performance of magnetic nanoparticles is not sufficient for cancer treatments, and therefore the surface of magnetic nanoparticles must be functionalized by ligands [22,23]. The general way to improve the surface modification and functionalization ability of magnetic nanoparticles is to coat each nanoparticle with a SiO_2 shell [23]. Optical transparency, highly biocompatibility, biodegradability, and manufacturability with porous surfaces make SiO_2 very useful as a biomaterial [24]. The study also includes understanding the effect of SiO_2 on the heating performance of $(Fe_{1-x},Ti_x)_3O_4$ nanoparticles. Although coating with SiO_2 has no effect on crystal structures, the SiO_2 thickness has caused a remarkable decrease in internal magnetization value of Fe_3O_4 [25]. One of the consequences of the reduction of internal magnetization can be observed as a decrease in the magneto heating performance of magnetic nanoparticles [26,27]. On the other hand, SiO_2 coating reduces interparticle interactions and inhibits aggregation, thereby increasing the heating capabilities of magnetic nanoparticles in AC fields [28–30]. Therefore, the magneto heating performance of magnetic nanoparticles is correlated with interacting or non-interacting particles [26–30].

The magnetic nanoparticles such as Fe_3O_4 seem as efficient nano-heaters in biomedical applications [31–33]. Surface modified $(Fe_{1-x},Ti_x)_3O_4$ nanoparticles are expected to be potential bio-materials which suitable for loading anticancer drugs and heating under both

excitations, RF magnetic field, and UV radiation, which utilize the magnetic nanoparticles useful at clinical hyperthermia applications.

2. Experimental

Magnetite nanoparticles were prepared via the co-precipitation method. Ferrous chloride tetrahydrate ($FeCl_2 \cdot 4H_2O$) and ferric chloride ($FeCl_3$) were used as iron precursors containing different valance states. On the other hand, Tetraisopropil Ortotinatate (TIPO) was used as a Titanium source. Natrium hydroxide (NaOH: 25% by weight) in H_2O and hydrochloric acid in water (HCl) were used as the precipitating agent. To prevent the agglomeration of magnetic nanoparticles, nanoparticles were coated with oleic acid at the end of the process. Ethanol and DI water were used to remove excessive coating agent. The schematic diagram of the procedure was demonstrated in Figure 1. The synthesis was performed on magnetic stirrer at 90 °C. Firstly, ferrous and ferric chloride iron salts were dissolved in water with HCl under Argon gas flow. Secondly, after half an hour, TIPO and NaOH were dropped into the solution. Oleic acid was added to the solution as the last step.
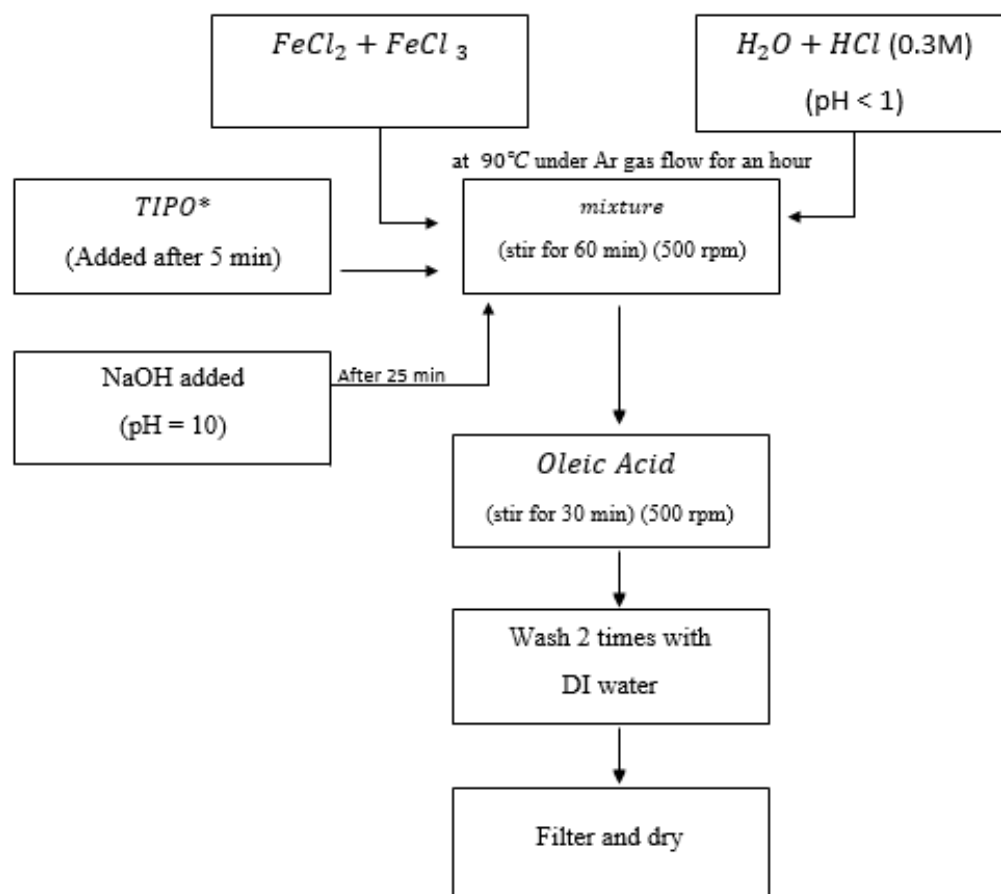

Figure 1. The schematic diagram of the synthesis procedure of pure and Ti-doped magnetite.

The coated nanoparticles were washed with DI water and ethanol to remove chloride ions and excessive coating materials. Furthermore, the same procedure was performed for the synthesis of the pure magnetite nanoparticles.

The nanoparticles were also coated with SiO_2 by base-catalyzed silica formation from tetraethylorthosilicate (TEOS) in a water-in-oil microemulsion technique, which was mentioned in previous study [34]. The resulting mixture was vigorously stirred for 24 h.

The crystal structures of samples were investigated by x-ray powder diffractometer (XRD), employing a MiniFlex model XRD, produced by Rigaku Corporation (Tokyo, Japan). The XRD patterns were taken under Cu K_α radiation (1.5406 Å) in 2θ range from 10°

to 90°. A JEM-2010F high-resolution transmission electron microscope (HR-TEM) (JEOL Ltd., Tokyo, Japan) was used to picture the structural morphologies of nanoparticles. Dc magnetization (σ (H)) measurements were performed at 300 K temperatures in a magnetic field range of $\pm$ 2 T.

Magneto-thermal characterization was taken by a homemade setup constructed using the equipment with a frequency of 150 kHz (power generator, thermometer, etc.). Experiments were performed in a custom-made setup with an alcohol thermometer, a covered glass tube, a water-cooled magnetic coil (diameter 50 mm and four turns for 160 Oe), and an AC power generator (Istanbul, Turkey) with a constant frequency of 150 kHz. The SAR measurements were conducted in non-adiabatic conditions as in many publications. The colloidal solution was put into a glass tube and the tube was placed in the coil. The thermometer was directly inserted into the solution. The temperature was measured using the thermometer as a function of time for a duration of 15 min. The filling level of the solution in the tube was adapted to the half-length of the coil to minimize the effects of magnetic field inhomogenity. Between the glass tube and the coils, we used styrofoam as an insulating material.

3. Result and Discussions

The structural analyses were performed employing XRD patterns for SiO_2 coated and uncoated particles as shown in Figure 2a,b respectively. The patterns were in an agreement with Fe_3O_4 diffraction pattern shown in ICDD card (PDF# 74-0748). No contamination or unexpected phase such as TiO_2 based structures, was detected on the XRD patterns. As seen in Figure 2b, even though having high background intensity, originating from the amorphous phase of SiO_2, the Fe_3O_4 patterns were distinctly distinguished at each XRD pattern.
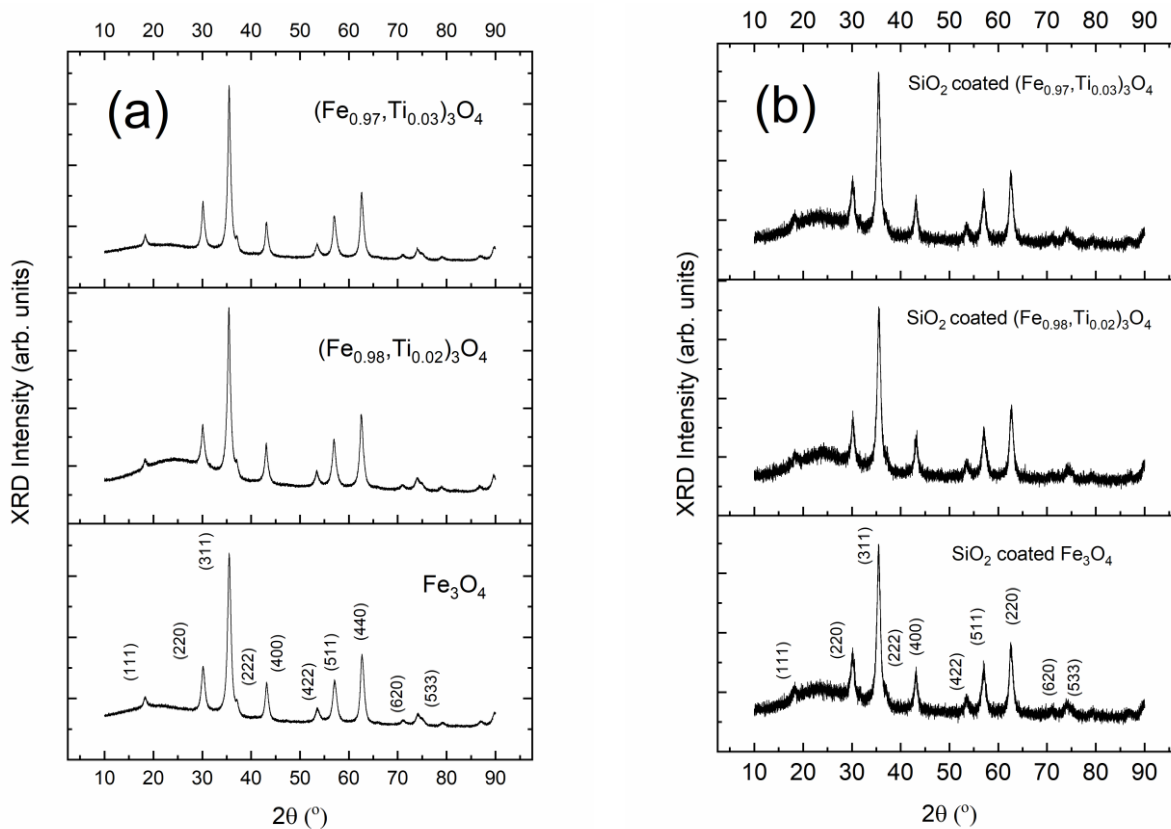

Figure 2. The XRD patterns of (**a**) Ti-doped magnetite and (**b**) SiO_2 coated Ti-doped magnetite.

Not observing Ti elements or compounds in the xrd patterns indicated the displacement of Ti atoms inside of Fe_3O_4 lattice. The ionic radius of Ti^{4+} is approximately 0.61Å, which is close to the ionic radius of Fe^{3+} (0.64 Å). Thus, Ti^{4+} ions are expected to settle instead of by Fe^{3+} ions in the octahedral lattice sites. Due to charge neutrality, a Ti^{4+} ion replacement in an octahedral site gives rise to change the valence state of Fe^{3+} ion to Fe^{2+} ion as shown in the chemical equation of (1) [35]. Due to its charge neutrality, the substitution of Ti^{4+}, a tetravalent positive ion, causes an Fe^{3+} ion to change its valency into Fe^{2+}. Chemical Equations (1) and (2) assign the charge neutrality occurring in $(Fe_{1-x},Ti_x)_3O_4$ lattice.

$$Fe^{2+} \leftrightarrow Fe^{3+} + e^- \tag{1}$$

$$2Fe^{3+} \rightarrow Ti^{4+} + Fe^{2+} \tag{2}$$

Increase in Ti^{4+} substitution amount ($0.01 \leq x \leq 0.025$) in $(Fe_{1-x},Ti_x)_3O_4$ lattice cause to formation of $Fe^{2+}{}_A(Fe^{2+}, Ti^{4+})_BO_4$ (A, tetrahedral side; B, octahedral side), which inhibits the hopping mechanism between iron ionic states. And thus, the new configuration cause to increase in magnetic anisotropy as mentioned in literature [35,36]. Excessive Ti^{4+} substitution ($x \geq 0.025$) easily bypasses Fe^{2+} ions, resulting in the formation of differential vacancies [35].

After understanding the crystal structure and possible defects in a lattice, the particle size distributions were investigated employing TEM micrographs. TEM Figures assigned homogeny distributed nanoparticles. In addition, due to covering with oleic acid, no agglomeration across the entire particle distribution was realized as seen in Figure 3.
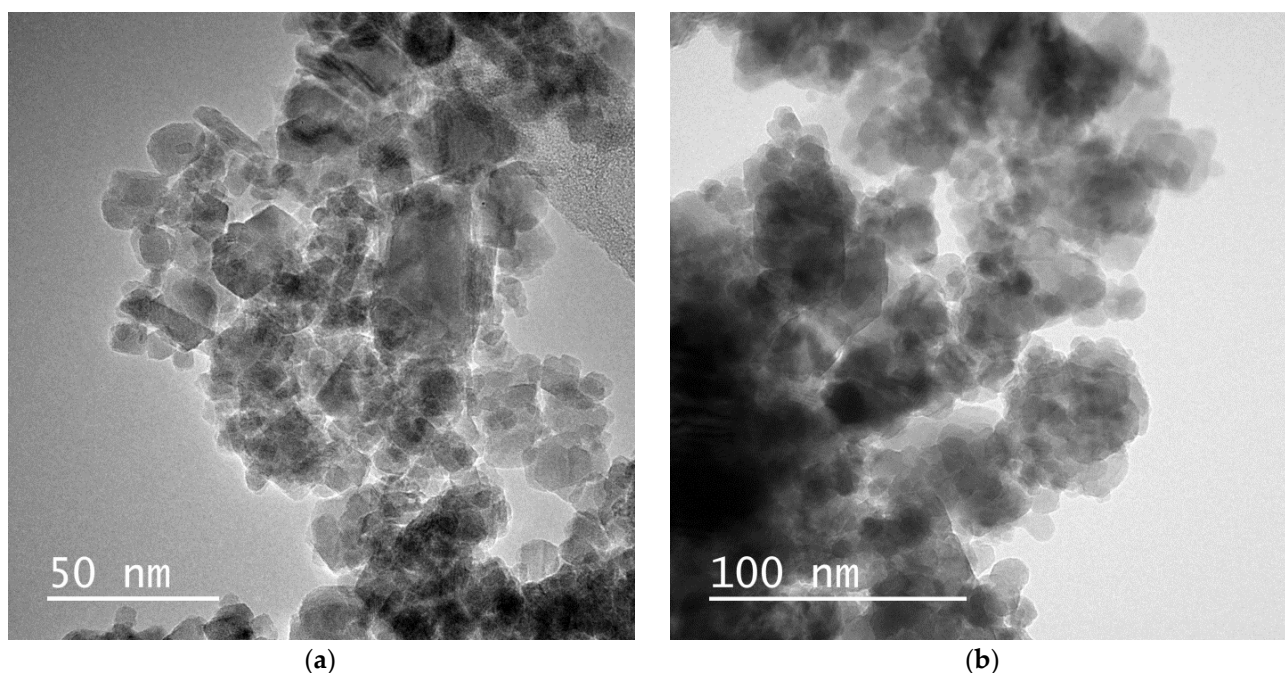

(**a**)   (**b**)

Figure 3. TEM micrographs of (**a**) uncoated and (**b**) coated $(Fe_{0.97},Ti_{0.03})_3O_4$ nanoparticles.

The size frequencies of particles were calculated by the subprogram of Image-J2. Particles with high differences in particle size were selected in the calculations. As shown on Figure 4, the particles size distributions which were confirmed by ImageJ, were found as 10.3 ± 0.6 nm and 18.7 ± 0.5 nm for uncoated and coated $(Fe_{0.97},Ti_{0.03})_3O_4$, respectively. The particles' size distribution indicated that the particles were in superparamagnetic regions.

The magnetization (σ (H)) measurements at the room temperature were illustrated in the Figure 5 for both samples uncoated and coated $(Fe_{1-x},Ti_x)_3O_4$. As seen from the Figure, the zero remanent magnetization assign the overcoming thermal energy to the magnetic anisotropy energy barrier at all samples. For both coated and uncoated $(Fe_{1-x},Ti_x)_3O_4$

particles, only difference in magnetization curves was the decrease in magnetization value by Ti amount in lattice. In order to understand the magnetic domain states of particles, room temperature magnetic hysteresis curves were obtained as shown in Figure 5.
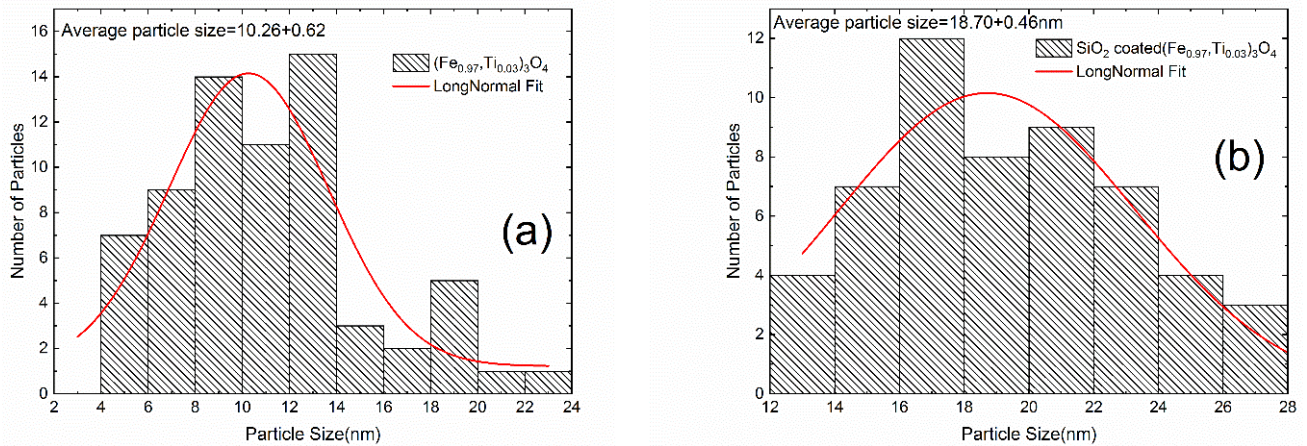

Figure 4. Calculated size distributions of (**a**) uncoated and (**b**) coated $(Fe_{0.97},Ti_{0.03})_3O_4$ nanoparticles via ImageJ subprogram.
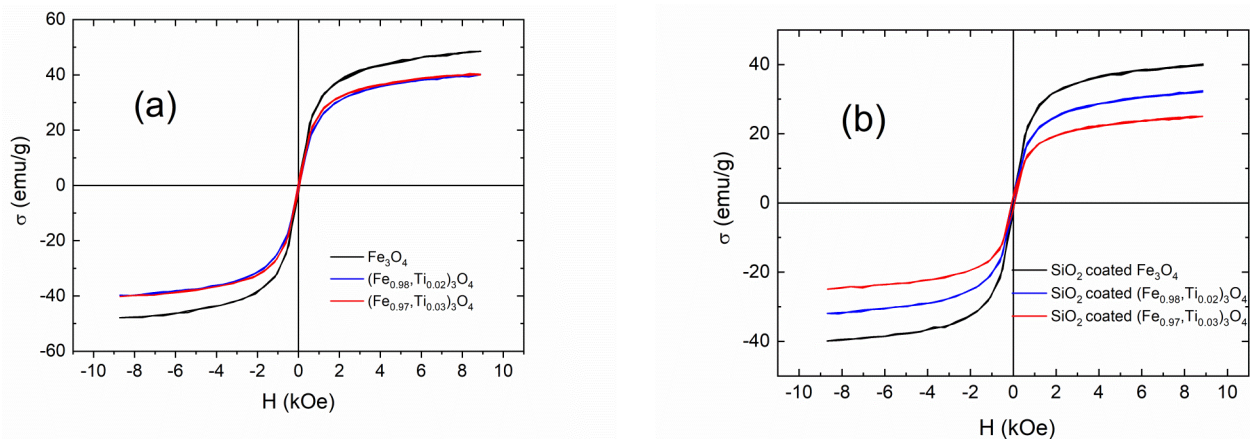

Figure 5. The magnetization measurements of (**a**) uncoated and (**b**) SiO$_2$ coated pure and Ti-doped magnetite.

Not observing coercivity and remanence values on hysteresis curves at room temperature proved that the particles were in superparamagnetic states [37,38]. Heating performance of an individual, non-interacting, and monodisperse particles have high SAR value due to dominating of Néel relaxation in a highly viscous environment. In the superparamagnetic state at room temperature, the magnetic interaction decreased to the lowest values with the effect of thermal energy. Nanoparticle size, anisotropy and interparticle interaction are the principal factors that influence heat generation [39,40]. Moreover, agglomerations between the magnetic nanoparticles occur due to strong magnetic dipole–dipole interactions between particles. As seen in Figure 5, coating with SiO$_2$ and doping with Ti atoms reduced the magnetization of the particles. A possible mechanism reducing the magnetization of particles is the number of vacancies in the crystal structure. The vacancies may form non-magnetic regions on the particle surface [41]. In addition, the magnetic anisotropy of the easy-axis is another parameter affecting the magnetization values that can be different either parallel or perpendicular to the easy-axis orientation of the domains [42]. These parameters manage the SAR values of particles.

Being predominant of thermal energy to magnetic energy at room temperature indicated that the nanoparticles were in superparamagnetic region. Since the particles were in

superparamagnetic state size, the Néel magnetic relaxation was expected to dominate the magneto heating performance of the particles.

In Figure 6, the heating performance of particles was investigated under an ac magnetic field, approximately 13 kA/m field intensity and frequency of 150 kHz (the biological limits are 5×10^9 A/(m.s). The magneto heating measurements were taken immediately after arranging nanoparticles as magnetic fluids in 1 ml ethanol media. As seen on the Figure, the temperature difference (ΔT) reach up to 30 °C for pure Fe_3O_4 and for the same time interval Ti doping lowered the ΔT value down to 20 °C (($Fe_{0.97}$,$Ti_{0.03}$)$_3O_4$ nanoparticles). For ($Fe_{0.97}$,$Ti_{0.03}$)$_3O_4$ nanoparticles, the ΔT value was measured as 22 °C, which was good enough for use in vivo studies.
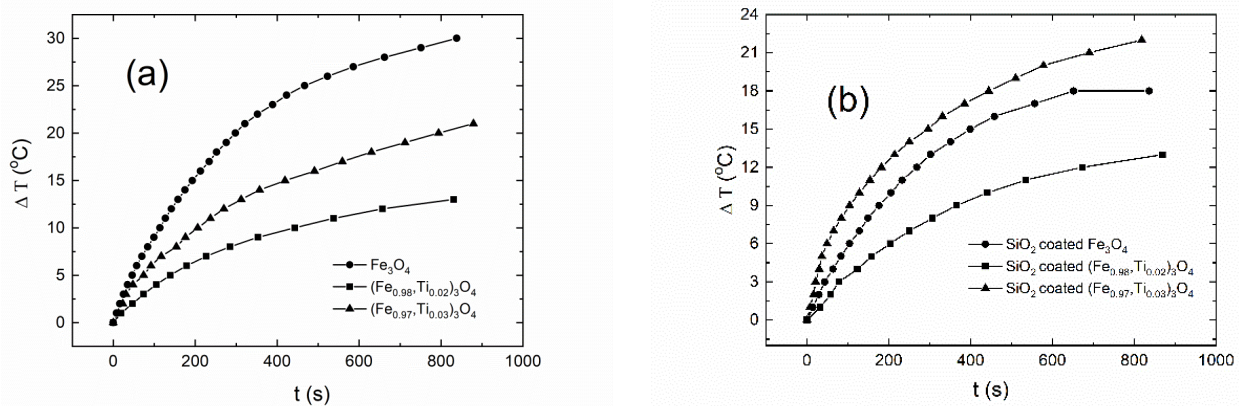

Figure 6. The magnetic heating performance of (**a**) uncoated and (**b**) SiO_2 coated pure and Ti doped Fe_3O_4.

Then, for each particle, the SAR value was calculated as shown in Table 1. The physical quantity of SAR value was determined by defined as the heat released from colloidal magnetic nanoparticles in unit time by Equation (3) [43].

$$SAR = \frac{Q}{\Delta t \; m_{mag}} \tag{3}$$

where $Q = mc\Delta T$, m_{mag} is the mass of magnetic nanoparticle, c is the specific heat of the colloid (only ethanol is taken into account, the contribution of magnetic nanoparticles, oleic acid, and SiO_2 to the specific heat are neglected). The calculations were performed for the heat capacity and the density of ethanol 2.57 kJ/(kgK), 0.789 g/mL, respectively.

Table 1. SAR values of (Fe_{1-x},Ti_x)$_3O_4$ (x = 0.00, 0.02 and 0.03) nanoparticles.

Nanoparticles	SAR (W/g)
Fe_3O_4	155
x = 0.02	70
x = 0.03	3
SiO_2 coated Fe_3O_4	104
x = 0.02 (SiO_2 coated)	34
x = 0.03 (SiO_2 coated)	116

The SAR values were illustrated in Table 1. As understood from Table 1, coating with SiO_2 lowered the SAR values of (Fe_{1-x},Ti_x)$_3O_4$ nanoparticles. However, for SiO_2 coated samples increase in Ti^{4+} ions amount in lattice caused an increase in SAR value, which getting closer to the value of pure Fe_3O_4 nanoparticles.

4. Conclusions

In the study, homogeny size distributed $(Fe_{1-x},Ti_x)_3O_4$ ferrite nanoparticles in oleic acid and at SiO_2 matrix were synthesized via a chemical route. The particles were obtained as superparamagnetic Fe_3O_4 nanoparticles to dominate the Néel relaxation over Brownian relaxation mechanism. Furthermore, lowering the particle size down to superparamagnetic region, coating with SiO_2 and Ti doping into the lattice was the tuned parameters to produce individual, non-interacting, and monodisperse particles. Then, the heating mechanism of SiO_2 coated Ti doped Fe_3O_4 nanoparticles were only correlated with Ti atoms amount in the lattice. Due to the expected coupling between Ti^{4+}-Fe^{2+} ions in the octahedral site, the heating performance by Ti doping was lower than pure Fe_3O_4. On the other hand, for SiO_2 coated $(Fe_{0.97},Ti_{0.03})_3O_4$ nanoparticles, the increase in the amount of Ti^{4+} ions in lattice cause an increase in SAR value ($\Delta T = 22\ °C$ in 10 min), while decreasing for uncoated nanoparticles. The heating performance of $(Fe_{0.97},Ti_{0.03})_3O_4$ nanoparticles coated with SiO_2 was almost close to the heating performance of pure magnetite.

Author Contributions: Conceptualization, M.M.C.; methodology, M.M.C.; formal analysis, M.M.C.; investigation, M.M.C., D.S.K., Z.A. and M.O.Ö.; resources, M.M.C.; data curation, M.M.C., C.B. and S.A.; writing—original draft preparation, M.M.C.; writing—review and editing, M.M.C., S.A., D.S.K., S.K., Z.A. and M.O.Ö.; visualization, M.M.C.; supervision, M.M.C.; project administration, M.M.C.; All authors have read and agreed to the published version of the manuscript.

Institutional Review Board Statement: Not applicable.

Informed Consent Statement: Not applicable.

Data Availability Statement: Data sharing is not applicable to this article.

Conflicts of Interest: The authors declare no conflict of interest.

References

1. Can, M.M.; Coşkun, M.; Fırat, T. Domain state-dependent magnetic formation of Fe_3O_4 nanoparticles analyzed via magnetic resonance. *J. Nanopart Res.* **2011**, *13*, 5497. [CrossRef]
2. Can, M.M.; Ozcan, S.; Fırat, T. Magnetic behaviour of iron nanoparticles passivated by oxidation. *Phys. Stat. Sol. C* **2006**, *3*, 1271–1278. [CrossRef]
3. Fortin, J.-P.; Gazeau, F.; Wilhelm, C. Intracellular heating of living cells through Néel relaxation of magnetic nanoparticles. *Eur. Biophys. J.* **2008**, *37*, 223–228. [CrossRef] [PubMed]
4. Jeyasubramanian, K.; Selvakumar, N.; Ilakkiya, J.; Santhoshkumar, P.; Satish, N.; Sahoo, S.K. Magnetic Flux Alignment Studies on Entrapped Ferrofluid Nanoparticles in Poly Vinyl Alcohol Matrix. *J. Mater. Sci. Technol.* **2013**, *29*, 903–908. [CrossRef]
5. Hilger, I.; Hergt, R.; Kaiser, W.A. Towards breast cancer treatment by magnetic heating. *J. Magn. Magn. Mater.* **2005**, *293*, 314–319. [CrossRef]
6. Nikam, D.S.; Jadhav, S.V.; Khot, V.M.; Phadatare, M.R.; Pawar, S.H. Study of AC magnetic heating characteristics of $Co_{0.5}Zn_{0.5}Fe_2O_4$ nanoparticles for magnetic hyperthermia therapy. *J. Magn. Magn. Mater.* **2014**, *349*, 208–213. [CrossRef]
7. Ortega, D.; Pankhurst, Q.A. *Magnetic Hyperthermia, in Nanoscience: Volume 1: Nanostructures through Chemistry*; O'Brien, P., Ed.; Royal Society of Chemistry: Cambridge, UK, 2013; pp. 60–88.
8. Périgo, E.A.; Hemery, G.; Sandre, O.; Ortega, D.; Garaio, E.; Plazaola, F.; Teran, F.J. Fundamentals and advances in magnetic hyperthermia. *Appl. Phys. Rev.* **2015**, *2*, 041302. [CrossRef]
9. Suto, M.; Hirota, Y.; Mamiya, H.; Fujita, A.; Kasuya, R.; Tohji, K.; Jeyadevan, B. Heat dissipation mechanism of magnetite nanoparticles in magnetic fluid hyperthermia. *J. Magn. Magn. Mater.* **2009**, *321*, 1493–1496. [CrossRef]
10. Obaidat, I.M.; Issa, B.; Haik, Y. Magnetic Properties of Magnetic Nanoparticles for Efficient Hyperthermia. *Nanomaterials* **2015**, *5*, 63–89. [CrossRef]
11. Dennis, C.L.; Ivkov, R. Physics of heat generation using magnetic nanoparticles for hyperthermia. *Int. J. Hyperth.* **2013**, *29*, 715–729. [CrossRef]
12. Verges, M.A.; Costo, R.; Roca, A.G.; Marco, J.F.; Goya, G.F.; Serna, C.J.; Morales, M.P. Uniform and water stable magnetite nanoparticles with diameters around the monodomain–multidomain limit. *J. Phys. D Appl. Phys.* **2008**, *41*, 134003. [CrossRef]
13. Skumiel, A.; Kaczmarek-Klinowska, M.; Timko, M.; Molcan, M.; Rajnak, M. Evaluation of Power Heat Losses in Multidomain Iron Particles under the Influence of AC Magnetic Field in RF Range. *Int. J. Thermophys.* **2013**, *34*, 655–666. [CrossRef]
14. Deatsch, A.E.; Evans, B.A. Heating efficiency in magnetic nanoparticle hyperthermia. *J. Magn. Magn. Mater.* **2014**, *354*, 163–172. [CrossRef]

15. Ilg, P.; Kröger, M. Dynamics of interacting magnetic nanoparticles: Effective behavior from competition between Brownian and Néel relaxation. *Phys. Chem. Chem. Phys.* **2020**, *22*, 22244–22259. [CrossRef] [PubMed]

16. Çelik, Ö.; Can, M.M.; Firat, T. Size dependent heating ability of $CoFe_2O_4$ nanoparticles in AC magnetic field for magnetic nanofluid hyperthermia. *J. Nanopart. Res.* **2014**, *16*, 232. [CrossRef]

17. Ganguly, S.; Margel, S. Review: Remotely controlled magneto-regulation of therapeutics frommagnetoelastic gel matrices. *Biotechnol. Adv.* **2020**, *44*, 1076112. [CrossRef] [PubMed]

18. Fannin, P.C.; Charles, S.W. The study of a ferrofluid exhibiting both Brownian and Néel relaxation. *J. Phys. D Appl. Phys.* **1989**, *22*, 187. [CrossRef]

19. Fannin, P.C.; Charles, S.W. On the calculation of the Néel relaxation time in uniaxial single-domain ferromagnetic particles. *J. Phys. D Appl. Phys.* **1994**, *27*, 185. [CrossRef]

20. Hergt, R.; Dutz, S.; Zeisberger, M. Validity limits of the Néel relaxation model of magnetic nanoparticles for hyperthermia. *Nanotechnology* **2010**, *21*, 015706. [CrossRef]

21. Fabris, F.; Lima, E.; Biasi, E.; Troiani, H.E.; Mansilla, M.V.; Torres, T.E.; Pacheco, R.F.; Ibarra, M.R.; Goya, G.F.; Zysler, R.D.; et al. Controlling the dominant magnetic relaxation mechanisms for magnetic hyperthermia in bimagnetic core–shell nanoparticles. *Nanoscale* **2019**, *11*, 3164–3172. [CrossRef]

22. Cole, A.J.; Yang, V.C.; David, A.E. Cancer theranostics: The rise of targeted magnetic nanoparticles. *Trends Biotechnol.* **2011**, *29*, 323–332. [CrossRef]

23. Schladt, T.D.; Schneider, K.; Schild, H.; Tremel, W. Synthesis and bio-functionalization of magnetic nanoparticles for medical diagnosis and treatment. *Dalton Trans.* **2011**, *40*, 6315–6343. [CrossRef] [PubMed]

24. Marcelo, G.A.; Lodeiro, C.; Capelo, J.L.; Lorenzo, J.; Oliveira, E. Magnetic, fluorescent and hybrid nanoparticles: From synthesis to application in biosystems. *Mater. Sci. Eng. C* **2020**, *106*, 110104. [CrossRef] [PubMed]

25. Husain, H.; Hariyanto, B.; Sulthonul, M.; Klysubun, W.; Darminto, D.; Pratapa, S. Structure and magnetic properties of silica-coated magnetitenanoparticle composites. *Mater. Res. Express* **2019**, *6*, 86117.

26. Lemal, P.; Balog, S.; Geers, C.; Taladriz-Blanco, P.; Palumbo, A.; Hirt, A.M.; Rothen-Rutishauser, B.; Petri-Fink, A. Heating behavior of magnetic iron oxide nanoparticles at clinically relevant concentration. *J. Magn. Magn. Mater.* **2019**, *474*, 637–642. [CrossRef]

27. Larumbe, S.; Gomez-Polo, C.; Perez-Landazabal, J.I.; Pastor, J.M. Effect of a SiO_2 coating on the magnetic properties of Fe_3O_4 nanoparticles. *J. Phys. Condens. Matter.* **2012**, *24*, 266007. [CrossRef]

28. Arteaga-Cardona, F.; Rojas-Rojas, K.; Costo, R.; Mendez-Rojas, M.A.; Hernando, A.; Presa, P. Improving the magnetic heating by disaggregating nanoparticles. *J. Alloy. Compd.* **2016**, *663*, 636–644. [CrossRef]

29. Ota, S.; Takemura, Y. Characterization of Néel and Brownian Relaxations Isolated from Complex Dynamics Influenced by Dipole Interactions in Magnetic Nanoparticles. *J. Phys. Chem. C* **2019**, *123*, 28859–28866. [CrossRef]

30. Kusigerski, V.; Illes, E.; Blanusa, J.; Gyergyek, S.; Boskovic, M.; Perovic, M.; Spasojevic, V. Magnetic properties and heating efficacy of magnesium doped magnetite nanoparticles obtained by co-precipitation method. *J. Magn. Magn. Mater.* **2019**, *475*, 470–478. [CrossRef]

31. Lak, A.; Disch, S.; Bende, P. Embracing Defects and Disorder in Magnetic Nanoparticles. *Adv. Sci.* **2021**, *8*, 2002682. [CrossRef]

32. Lavorato, G.C.; Das, R.; Masa, J.A.; Phan, M.-H.; Srikanth, H. Hybrid magnetic nanoparticles as efficient nano heaters in biomedical applications. *Nanoscale Adv.* **2021**, *3*, 867–888. [CrossRef]

33. Sharifianjazi, F.; Irani, M.; Esmaeilkhanian, A.; Bazli, L.; Asl, M.S.; WonJang, H.; Kim, S.Y.; Ramakrishna, S.; Shokouhimehr, M.; Varma, R.S. Polymer incorporated magnetic nanoparticles: Applications for agnetoresponsive targeted drug delivery. *Mater. Sci. Eng. B* **2021**, *272*, 115358. [CrossRef]

34. Coskun, M.; Can, M.M.; Duyar-Coskun, Ö.; Korkmaz, M.; Fırat, T. Surface anisotropy change of $CoFe_2O_4$ nanoparticles depending on thickness of coated SiO_2 shell. *J. Nanopart. Res.* **2012**, *14*, 1197. [CrossRef]

35. Walz, F.; Torres, L.; Bendimya, K.; Francisco, C.; Kronmuller, H. Analysis of magnetic after-effect spectra in titanium-doped magnetite. *Phys. Status Solidi* **1997**, *164*, 805. [CrossRef]

36. Kakol, Z.; Sabol, J.; Stickler, J.; Kozfowski, A.; Honig, J.M. Influence of titanium doping on the magneto crystalline anisotropy of magnetite. *Phys. Rev. B* **1994**, *49*, 12767–12772. [CrossRef]

37. Petracic, O. Superparamagnetic nanoparticle ensembles. *Superlattices Microstruct.* **2010**, *47*, 569–578. [CrossRef]

38. Kim, D.K.; Zhang, Y.; Voit, W.; Rao, K.V.; Muhammed, M. Synthesis and characterization of surfactant-coated superparamagnetic monodispersed iron oxide nanoparticles. *J. Magn. Magn. Mater.* **2001**, *225*, 30–36. [CrossRef]

39. Lasheras, X.; Insausti, M.; Fuente, J.M.; Muro, I.G.; Castellanos-Rubio, I.; Marcano, L.; Fernández-Gubieda, M.L.; Serrano, A.; Martín-Rodríguez, R.; Garaio, E.; et al. Mn-Doping level dependence on the magnetic response of $Mn_xFe_{3x}O_4$ ferrite nanoparticles. *Dalton Trans.* **2019**, *48*, 11480–11491. [CrossRef]

40. Usov, N.A.; Serebryakova, O.N.; Tarasov, V.P. Interaction Effects in Assembly of Magnetic Nanoparticles. *Nanoscale Res. Lett.* **2017**, *12*, 489. [CrossRef]

41. Köhler, T.; Feoktystov, A.; Petracic, O.; Kentzinger, E.; Bhatnagar-Schöffmann, T.; Feygenson, M.; Nandakumaran, N.; Landers, J.; Wende, H.; Cervellino, A.; et al. Mechanism of magnetization reduction in iron oxide nanoparticles. *Nanoscale* **2021**, *13*, 6965–6976. [CrossRef]

42. Yamaminami, T.; Ota, S.; Trisnanto, S.B.; Ishikawa, M.; Yamada, T.; Yoshida, T.; Enpuku, K.; Takemura, Y. Power dissipation in magnetic nanoparticles evaluated using the AC susceptibility of their linear and nonlinear responses. *J. Magn. Magn. Mater.* **2021**, *517*, 167401. [CrossRef]

43. Rosensweig, R.E. Heating magnetic fluid with alternating magnetic field. *J. Magn. Magn. Mater.* **2002**, *252*, 370–374. [CrossRef]